Electronic Supplementary Material (ESI) for Inorganic Chemistry Frontiers.

Electronic Supplementary Information

Geometric Isomers of Asymmetric Rigid Four-Membered Chelating Ring Based Deep-Red-Emitting Iridium Complexes Fea-turing Three Charged (0, -1, -2) Ligands

Ruoqi Zeng,[1] Nengquan Li,[2] Feiyang Li,[1] Chao Shi,[1]* Zhen Jiang,[1] Fuzheng Zhang,[1] Qiuxia Li,[1]* Kaishun Ye,[1] Aihua Yuan,[1]* and Chuluo Yang,[2]*

[1] School of Environmental and Chemical Engineering, Jiangsu University of Science and Technology, Zhenjiang 212003, P. R. China.

[2] College of Materials Science and Engineering, Shenzhen University, Shenzhen 518060, P. R. China.

Corresponding Authors' E-mail address

* shichao@just.edu.cn
* liqiuxia2019@just.edu.cn
* aihua.yuan@just.edu.cn
* clyang@szu.edu.cn

Contents:

General information

Unless noted, all reagents or solvents were obtained from commercial suppliers and used without further purification. All air sensitive experiments were performed in N_2 atmosphere through schlenk technology. The iridium(III) complex precursor compounds (**1a**, **2a** and **2b**) were synthesized according to literature procedures[1]. The ^{1}H NMR and ^{13}C NMR spectra were measured by using a Bruker 400 MHz or 600 MHz spectrometer at room temperature. Mass spectra were conducted at Agilent Technologies 5973N (EI). Elemental analyses for C, H, and N were performed on a Vario MICRO elemental analyzer. An Edinburgh FS5 spectrophotometer was used to measure phosphorescence spectra. An Edinburgh FLS-980 spectrometer was used to determine phosphorescence quantum efficiency and lifetimes of the molecule. The experiments for cyclic voltametric were performed by using three electrode cell assemblies from an IM6ex instrument (Zahner). A one-compartment cell equipped with a platinum wire counter electrode, a Ag/Ag^{+} reference electrode, and a glassy-carbon working electrode was used for all measurements with a scan rate of 100 mVs^{-1}. The concentration of tetrabutylammonium hexafluorophosphate (Bu_4NPF_6) in dichloromethane solution a was 0.10 $molL^{-1}$ and used as supporting electrolyte.

Synthesis and characterization

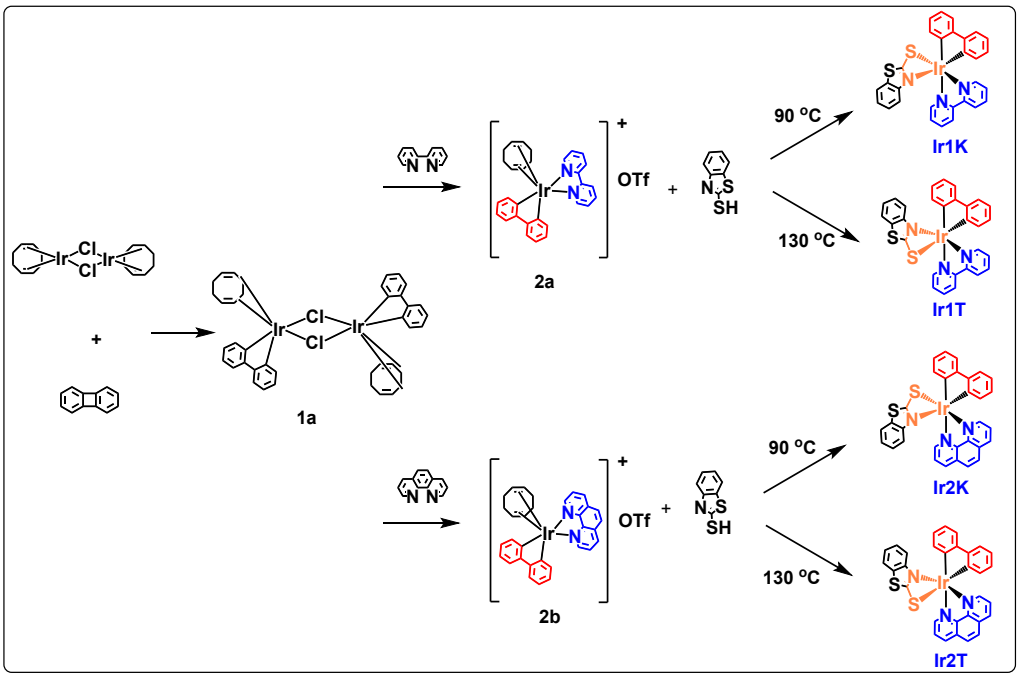

Figure S1. Synthetic route of the asymmetric rigid four-membered Ir-N-C-S chelating ring based iridium complexes isomers (**Ir1K**, **Ir1T**, **Ir2K** and **Ir2T**) featuring three charged (0, -1, -2) ligands.

Ir1K: 2a (0.039 g, 0.05 mmol), benzo[d]thiazole-2-thiol (0.010 g, 0.06 mmol) and Na_2CO_3 (0.013 g, 0.11 mmol) were charged to a 100 mL schlenck tube, followed by 2-ethoxyethanol (10 mL). The mixture was heated to 90 °C for 24 h under N_2. The resulting solution was saturated with water and extracted with CH_2Cl_2 three times. The combined organic phase was dried and concentrated in vacuum, and target product was purified by column chromatography on silica gel with CH_2Cl_2/ petroleum ether 5:1 (v/v) to afford red solid. 10 mg (30 %). ^{1}H NMR (600 MHz, DMSO-d_6) δ 9.51 (d, J = 5.6 Hz, 1H), 8.81 (d, J = 8.2 Hz, 1H), 8.62 (d, J = 8.1 Hz, 1H), 8.38 (m, 1H), 8.04 (m, 2H), 7.87 (m, 2H), 7.65 (d, J = 7.8 Hz, 1H), 7.46 (dd, J = 7.2, 2.0 Hz, 1H), 7.40 (m, 2H), 7.33 (d, J = 7.6 Hz, 1H), 7.25 (t, J = 7.7 Hz, 1H), 7.11 (t, J = 7.6 Hz, 1H), 6.97 (m, 2H), 6.68 (t, J = 7.4 Hz, 1H), 6.39 (t, J = 7.4 Hz, 1H), 5.61 (d, J = 7.5 Hz, 1H). ^{13}C NMR (151 MHz, DMSO-d_6) δ 175.7, 156.8, 156.4, 154.0, 153.7, 153.6, 153.1, 152.4, 147.9, 145.6, 139.9, 138.8, 137.0, 136.2, 131.0, 128.4, 127.6, 126.7, 125.8, 125.6, 124.5, 124.4, 123.4, 123.1, 122.9, 120.8, 120.6, 120.1, 118.8. $C_{29}H_{20}IrN_3S_2$ calcd: C, 52.23; N, 6.30; H, 3.02. Found: C, 52.20; N, 6.28; H, 3.09. EI-MS (*m/z*): 667.3 (M^+, 100%).

Ir1T: 2a (0.039 g, 0.05 mmol), benzo[d]thiazole-2-thiol (0.010 g, 0.06 mmol) and Na_2CO_3 (0.013 g, 0.11 mmol) were charged to a 100 mL schlenck tube, followed by 2-ethoxyethanol (10 mL). The mixture was

heated to 130 °C for 24 h under N_2. The resulting solution was saturated with water and extracted with CH_2Cl_2 three times. The combined organic phase was dried and concentrated in vacuum, and target product was purified by column chromatography on silica gel with CH_2Cl_2/ petroleum ether 5:1 (v/v) to afford red solid. 23 mg (69 %). ^{1}H NMR (400 MHz, $CDCl_3$) δ 8.43 (m, 1H), 8.24 (m, 2H), 8.20 (d, J = 8.1 Hz, 1H), 8.03 (td, J = 7.9, 1.6 Hz, 1H), 7.96 (d, J = 7.4 Hz, 1H), 7.53 (m, 6H), 6.97 (m, 4H), 6.86 (m, 2H), 6.53 (td, J = 7.4, 1.4 Hz, 1H), 6.12 (dd, J = 7.4, 1.1 Hz, 1H), 5.99 (d, J = 7.6 Hz, 1H). ^{13}C NMR (101 MHz, $CDCl_3$) δ 194.7, 185.7, 155.1, 153.8, 138.6, 137.3, 136.8, 134.9, 132.2, 131.9, 127.6, 126.5, 126.3, 126.1, 124.7, 124.6, 124.5, 124.1, 123.6, 123.0, 122.8, 122.5, 122.4, 122.2, 120.5, 119.8, 119.7, 116.8, 116.1. $C_{29}H_{20}IrN_3S_2$ calcd: C, 52.23; N, 6.30; H, 3.02. Found: C, 52.19; N, 6.26; H, 3.11. EI-MS (*m/z*): 667.3 (M^+, 100%).

Ir2K: 2b (0.041 g, 0.05 mmol), benzo[d]thiazole-2-thiol (0.010 g, 0.06 mmol) and Na_2CO_3 (0.013 g, 0.11 mmol) were charged to a 100 mL schlenck tube, followed by 2-ethoxyethanol (10 mL). The mixture was heated to 90 °C for 24 h under N_2. The resulting solution was saturated with water and extracted with CH_2Cl_2 three times. The combined organic phase was dried and concentrated in vacuum, and target product was purified by column chromatography on silica gel with CH_2Cl_2/ petroleum ether 5:1 (v/v) to afford red solid. 8 mg (23 %). ^{1}H NMR (600 MHz, $CDCl_3$) δ 10.04 (dd, J = 5.0, 1.4 Hz, 1H), 8.80 (dd, J = 5.4, 1.3 Hz, 1H), 8.49 (dd, J = 8.2, 1.4 Hz, 1H), 8.20 (dd, J = 8.1, 1.3 Hz, 1H), 8.03 (m, 2H), 7.94 (d, J = 8.8 Hz, 1H), 7.62 (dd, J = 15.0, 7.7 Hz, 2H), 7.45 (m, 2H), 7.01 (m, 2H), 6.88 (qd, J = 7.8, 3.3 Hz, 3H), 6.67 (td, J = 7.4, 1.3 Hz, 1H), 6.33 (td, J = 7.3, 1.4 Hz, 1H), 5.91 (m, 2H). ^{13}C NMR (101 MHz, $CDCl_3$) δ 219.7, 187.9, 156.1, 154.6, 151.6, 149.8, 149.3, 147.5, 141.6, 135.9, 134.6, 133.5, 132.2, 132.1, 130.6, 130.3, 129.0, 127.7, 127.3, 126.4, 126.3, 125.7, 125.5, 124.3, 122.6, 122.5, 122.1, 121.2, 120.0, 119.6, 115.1. $C_{31}H_{20}IrN_3S_2$ calcd: C, 53.90; N, 6.08; H, 2.92. Found: C, 53.86; N, 6.06; H, 2.97. EI-MS (*m/z*): 691.2 (M^+, 100%).

Ir2T: 2a (0.041 g, 0.05 mmol), benzo[d]thiazole-2-thiol (0.010 g, 0.06 mmol) and Na_2CO_3 (0.013 g, 0.11 mmol) were charged to a 100 mL schlenck tube, followed by 2-ethoxyethanol (10 mL). The mixture was heated to 130 °C for 24 h under N_2. The resulting solution was saturated with water and extracted with CH_2Cl_2 three times. The combined organic phase was dried and concentrated in vacuum, and target product was purified by column chromatography on silica gel with CH_2Cl_2/ petroleum ether 5:1 (v/v) to afford red solid. 15 mg (43 %). ^{1}H NMR (400 MHz, $CDCl_3$) δ 8.60 (dd, J = 5.4, 1.2 Hz, 1H), 8.56 (dd, J = 5.0, 1.3 Hz, 1H), 8.49 (dd, J = 8.2, 1.1 Hz, 1H), 8.31 (m, 1H), 8.03 (dd, J = 16.1, 8.5 Hz, 2H), 7.89 (m,

2H), 7.54 (m, 1H), 7.49 (m, 2H), 7.30 (m, 1H), 7.02 (m, 3H), 6.85 (m, 2H), 6.40 (td, J = 7.3, 1.4 Hz, 1H), 6.07 (d, J = 7.7 Hz, 1H), 5.99 (dd, J = 7.5, 1.0 Hz, 1H). ^{13}C NMR (101 MHz, $CDCl_3$) δ 207.1, 183.2, 164.1, 154.9, 149.0, 142.4, 140.9, 137.7, 135.9, 134.2, 134.1, 132.3, 132.2, 131.6, 131.5, 127.5, 127.3, 126.4, 126.1, 125.3, 124.5, 123.6, 122.9, 122.8, 122.4, 122.0, 120.5, 119.8, 119.7, 117.1, 116.3. $C_{31}H_{20}IrN_3S_2$ calcd: C, 53.90; N, 6.08; H, 2.92. Found: C, 53.87; N, 6.04; H, 2.95. EI-MS (*m/z*): 691.3 (M^+, 100%).

X-ray crystal structure analysis

The single-crystals of **Ir1K**, **Ir1T** and **Ir2T** were all obtained by slow diffusion of ethanol to their CH_2Cl_2 solutions, respectively. The single-crystal of **Ir2K** was obtained by slow diffusion of ethanol to its $CHCl_3$ solution. The X-ray diffraction data were collected on a Bruker Smart CCD Apex DUO diffractometer with graphite monochromated Mo Kα radiation (λ = 0.71073 Å) using the ω-2θ scan mode. All crystal datas are deposited in The Cambridge Crystallographic Data Centre (CCDC: 2234483 for **Ir1K**, 2234484 for **Ir1T**, 2234485 for **Ir2K** and 2234486 for **Ir2T**).

Table S1. Crystallographic data for **Ir1K**, **Ir1T**, **Ir2K** and **Ir2T**.

Complex	**Ir1K**	**Ir1T**	**Ir2K**	**Ir2T**
chemical formula	$2(C_{29}H_{20}IrN_3S_2)$, CH_2Cl_2	$C_{29}H_{20}IrN_3S_2$	$C_{31}H_{20}IrN_3S_2$, $CHCl_3$	$C_{31}H_{20}IrN_3S_2$
formula weight	1418.52	666.80	810.19	690.82
crystal size (mm)	0.13 × 0.16 × 0.17	0.14 × 0.17 × 0.18	0.08 × 0.10 × 0.11	0.07 × 0.09 × 0.12
temperature (K)	200	150	100	150
radiation	0.71073	0.71073	0.71073	0.71073
crystal system	Triclinic	Tetragonal	Triclinic	Monoclinic
space group	P-1	I41/a	P-1	P21/n
a(Å)	9.4955(10)	17.6304(4)	10.0417(1)	9.7082(5)
b(Å)	11.7819(12)	17.6304(4)	10.1106(2)	19.5157(8)
c(Å)	14.2124(15)	35.1485(17)	16.2358(3)	15.0090(8)
α(°)	100.816(2)	90	99.343(1)	90
β(°)	108.292(1)	90	97.835(1)	97.881(2)
γ(°)	111.137(1)	90	113.684(2)	90

V(Å^3)	1324.4(2)	10925.2(7)	1452.00(5)	2816.8(2)
Z	1	16	2	4
$\rho_{(calc)}$ (g/cm^3)	1.779	1.622	1.853	1.629
F (000)	690	5184	788	1344
absorp.coeff. (mm^{-1})	5.324	5.063	5.047	4.912
θ range (deg)	1.6 to 25.0	2.1 to 26.4	2.3 to 25.0	2.4 to 25.0
reflns collected	9824 (R_{int} = 0.030)	119077 (R_{int} = 0.087)	23711 (R_{int} = 0.032)	37355 (R_{int} = 0.054)
indep. reflns	4574	5581	5089	4975
Refns obs.[$I>2\sigma(I)$]	4335	4703	4846	4332
data/restr/paras	4574/0/334	5581/0/316	5089/0/370	4975/0/334
GOF	1.20	1.11	1.03	1.24
R_1/wR_2 [$I>2\sigma(I)$]	0.0299/0.0874	0.0370/0.0905	0.0199/0.0433	0.0483/0.1144
R_1/wR_2 (all data)	0.0333/0.1059	0.0448/0.0947	0.0218/0.0441	0.0557/0.1177
larg peak and hole(e/Å^3)	1.70/–1.37	1.43/–1.91	0.86/–0.75	1.78/–1.08

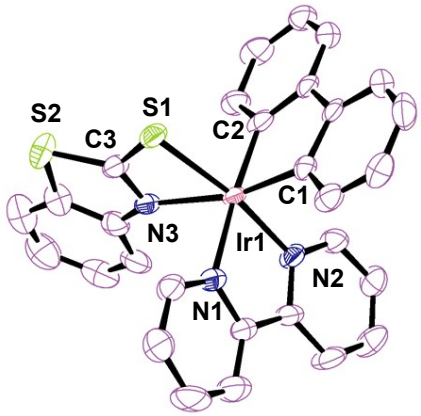

Ir1K

Figure S2. The single crystal structure of **Ir1K**, the hydrogen atoms have been omitted for clarity, selected bond lengths (Å) and angles (°): Ir1−C1: 2.000(7), Ir1−C2: 2.031(7), Ir1−N1: 2.135(6), Ir1−N2: 2.041(6), Ir1−S1: 2.379(2), Ir1−N3: 2.216(6), C3−S1: 1.713(7), C3−N3: 1.295(9), C3−S2: 1.748(7); C1–Ir1–C2: 80.7(3), N1–Ir1–N2: 78.7(2), N3–Ir1–S1: 67.37(16), N3–C3–S1: 115.3(5).

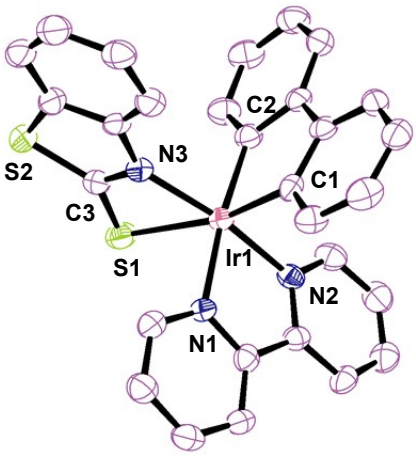

Ir1T

Figure S3. The single crystal structure of **Ir1T**, the hydrogen atoms have been omitted for clarity, selected bond lengths (Å) and angles (°): Ir1−C1: 2.022(5), Ir1−C2: 2.020(5), Ir1−N1: 2.110(4), Ir1−N2: 2.037(4), Ir1−S1: 2.5656(16), Ir1−N3: 2.058(4), C3−S1: 1.701(5), C3−N3: 1.318(6), C3−S2: 1.759(5); C1–Ir1–C2: 80.6(2), N1–Ir1–N2: 78.41(14), N3–Ir1–S1: 66.22(11), N3–C3–S1: 115.5(4).

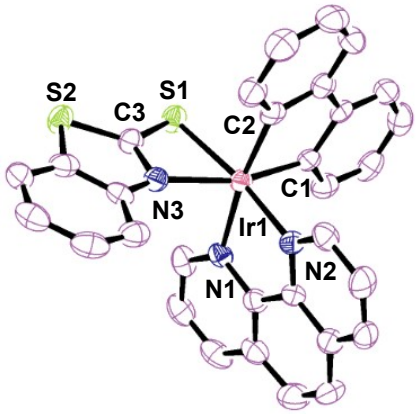

Ir2K

Figure S4. The single crystal structure of **Ir2K**, the hydrogen atoms have been omitted for clarity, selected bond lengths (Å) and angles (°): Ir1−C1: 2.016(3), Ir1−C2: 2.015(3), Ir1−N1: 2.131(3), Ir1−N2: 2.049(3), Ir1−S1: 2.377(9), Ir1−N3: 2.196(3), C3−S1: 1.720(3), C3−N3: 1.316(4), C3−S2: 1.734(3); C1–Ir1–C2: 81.66(12), N1–Ir1–N2: 79.04(11), N3–Ir1–S1: 67.92(8), N3–C3–S1: 114.3(2).

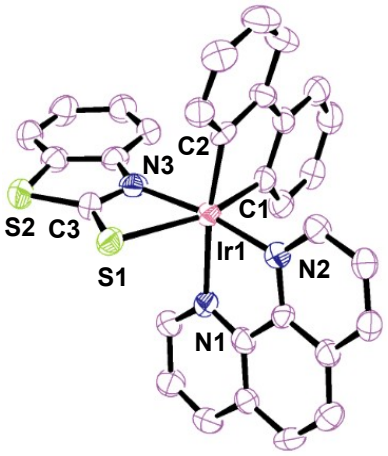

Ir2T

Figure S5. The single crystal structure of **Ir2T**, the hydrogen atoms have been omitted for clarity, selected bond lengths (Å) and angles (°): Ir1−C1: 2.019(9), Ir1−C2: 2.012(8), Ir1−N1: 2.185(8), Ir1−N2: 2.027(8), Ir1−S1: 2.586(2), Ir1−N3: 2.057(8), C3−S1: 1.699(10), C3−N3: 1.317(12), C3−S2: 1.741(10); C1–Ir1–C2: 80.7(3), N1–Ir1–N2: 78.6(3), N3–Ir1–S1: 65.7(2), N3–C3–S1: 115.5(7).

Photophysical and electrochemical properties

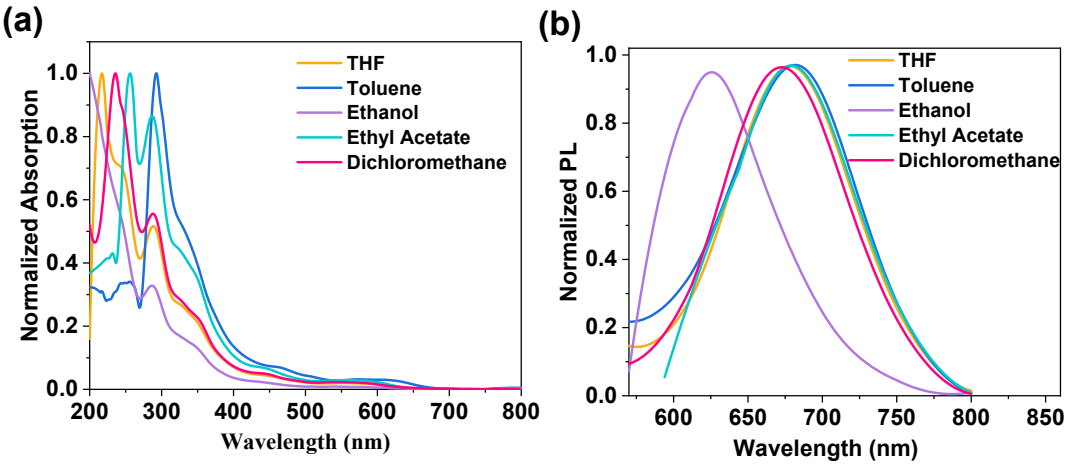

Figure S6. (a) Absorption and (b) PL spectra of the iridium complex **Ir1K** in different solutions.

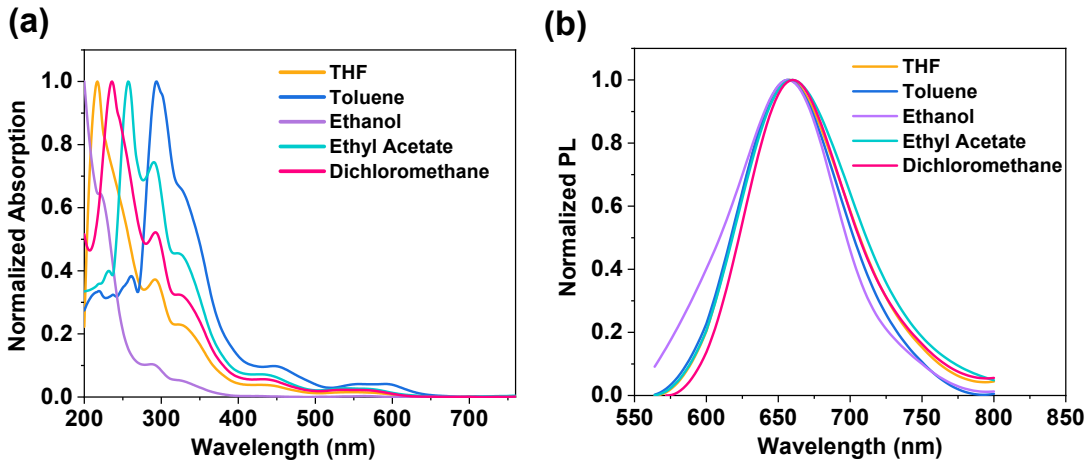

Figure S7. (a) Absorption and (b) PL spectra of the iridium complex **Ir1T** in different solutions.

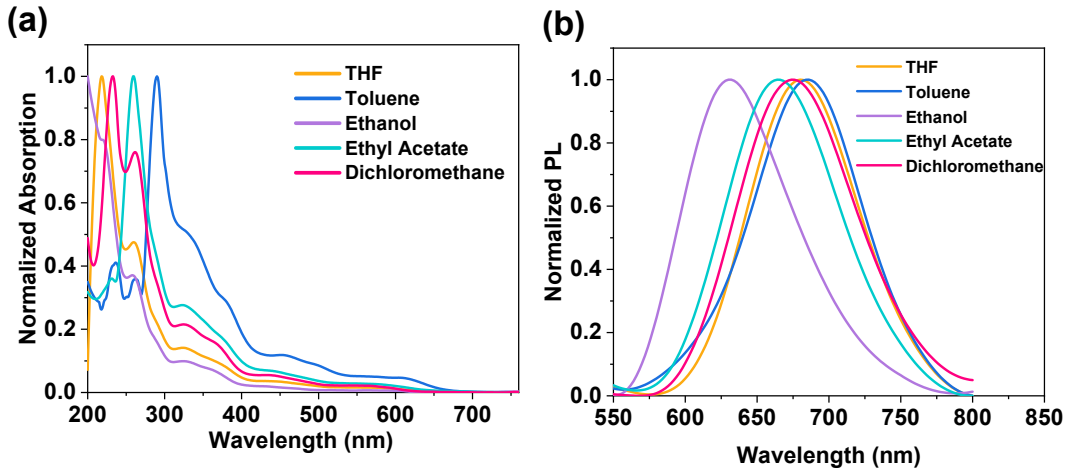

Figure S8. (a) Absorption and (b) PL spectra of the iridium complex **Ir2K** in different solutions.

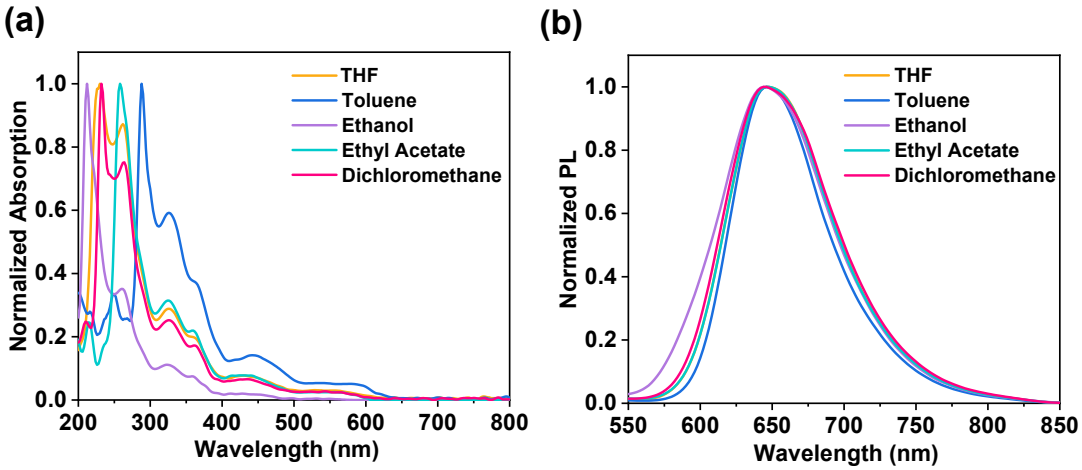

Figure S9. (a) Absorption and (b) PL spectra of the iridium complex **Ir2T** in different solutions.

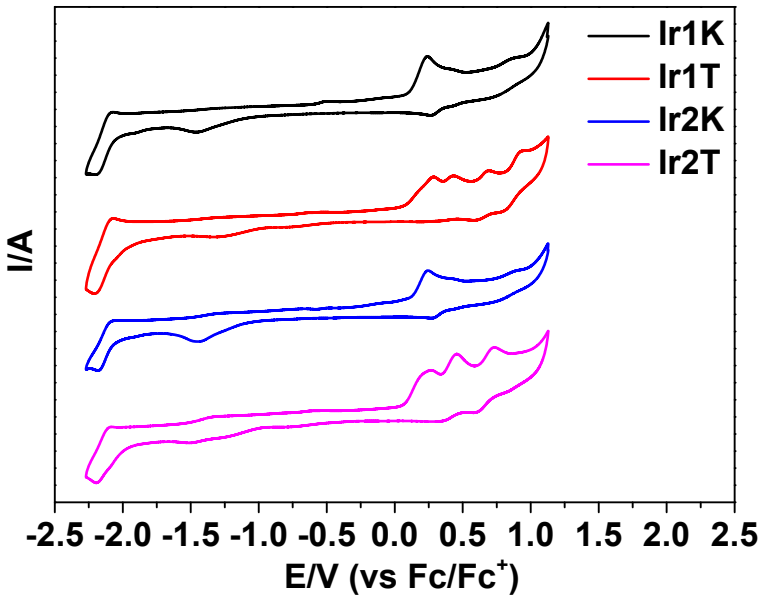

Figure S10. Cyclic voltammogram of the asymmetric four-membered Ir-N-C-S chelating ring based iridium complexes isomers (**Ir1K**, **Ir1T**, **Ir2K** and **Ir2T**) in dichloromethane under the scan rate of 100 mV s^{-1}.

TG analysis

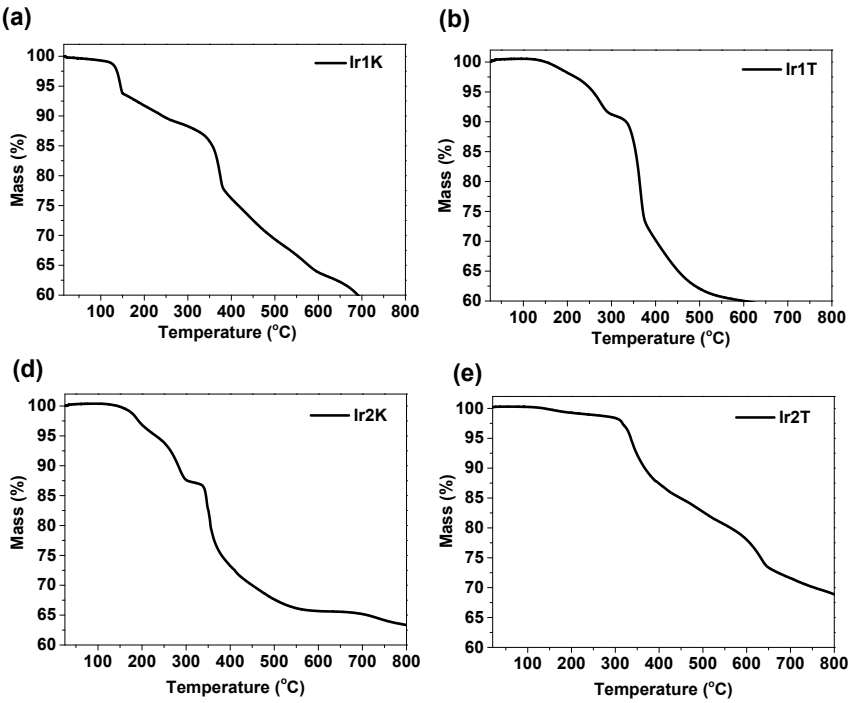

Figure S11. TG thermograms of the iridium complexes (a) **Ir1K**, (b) **Ir1T**, (c) **Ir2K** and (d) **Ir2T**.

DFT calculation

DFT method was used to optimize the geometries all the complexes. The electronic transition energies and electron correlation effects were also calculated by (TD)-DFT method with the B3LYP functional (TD-B3LYP). The LANL2DZ basis set was used to treat with the iridium atom, and the 6–31G(d) basis set was used to treat with all other atoms. The sum of electronic and zero-point energies (E_0) and the sum of electronic and thermal free energies (G) of all complexes were obtained by frequency calculation. The contributions of fragments to the ‘‘holes’’ and ‘‘electrons’’ and Inter Fragment Charge Transfer (IFCT) in the electronic excitation process were analyzed by the Hirshfeld method in the Multiwfn 3.8 program[2]. All calculations were carried out according to the Gaussian 09 program.[3]

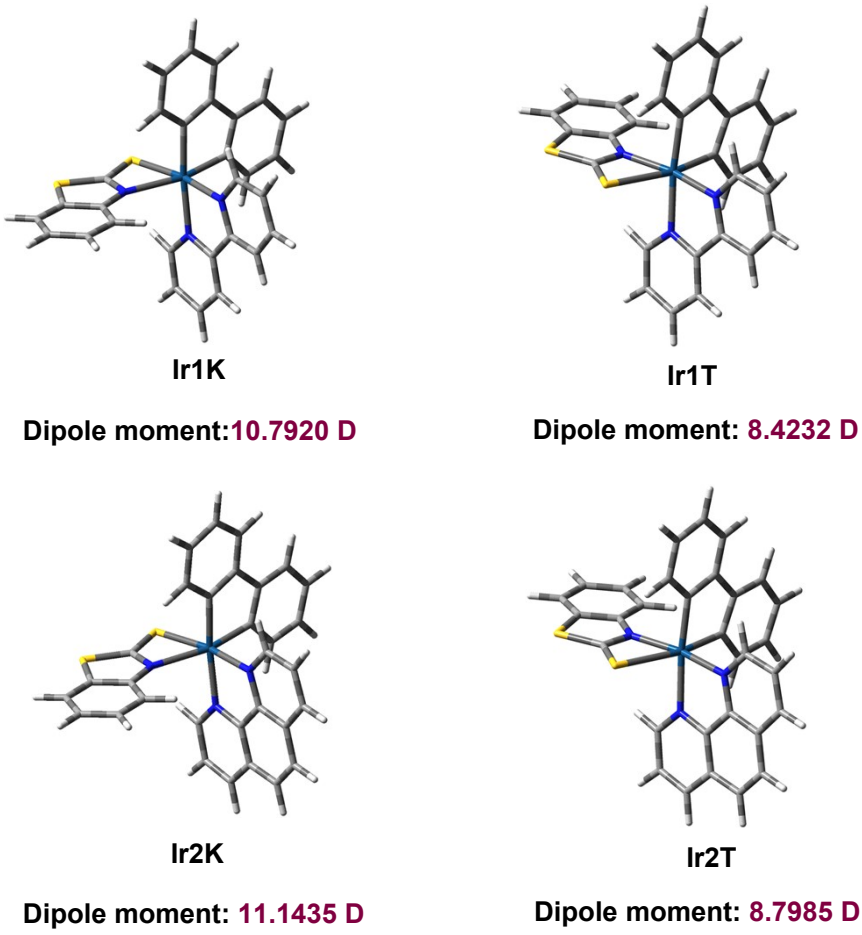

Figure S12. Optimized structures and dipole moment for **Ir1K**, **Ir1T**, **Ir2K** and **Ir2T** at the ground state (S_0).

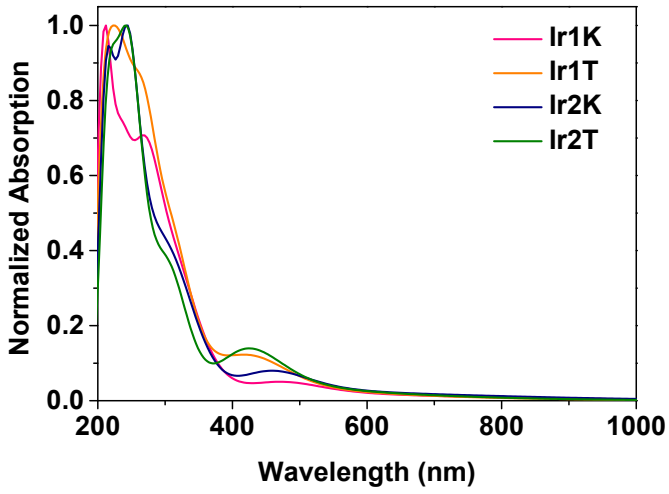

Figure S13. Calculated UV spectra of **Ir1K**, **Ir1T**, **Ir2K** and **Ir2T**.

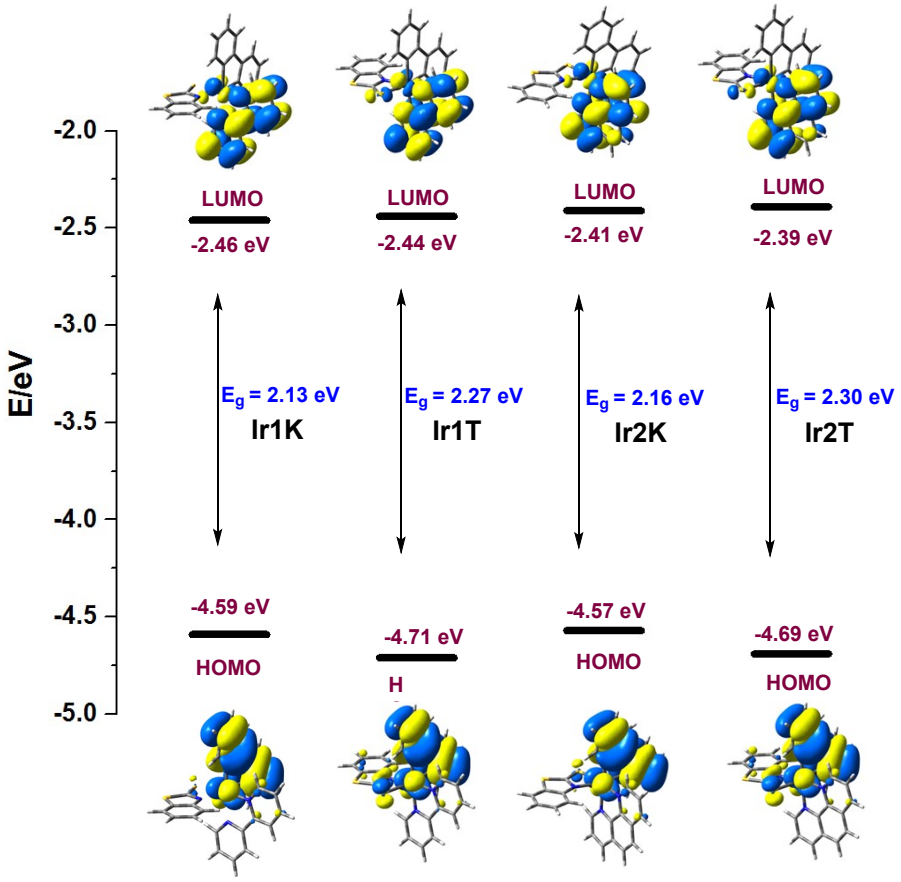

Figure S14. HOMO and LUMO spatial distribution and energy levels of all iridium complexes isomers at the ground state (S_0).

Table S2. Calculated energies and oscillator strengths for lowest-energy singlet (S_1) and triplet (T_1) transitions.

Complexes	states	E (eV)	Oscillator strength	main configurations (CI coeff)	Character
Ir1K	S_1	1.5013	0.0048	HOMO→LUMO (0.96)	MLCT/LLCT
	T_1	0.8885	0	HOMO→LUMO (0.96)	^{3}MLCT/^{3}LLCT
Ir1T	S_1	1.6164	0.0036	HOMO→LUMO (0.96)	MLCT/LLCT
	T_1	1.0748	0	HOMO→LUMO (0.96)	^{3}MLCT/^{3}LLCT
Ir2K	S_1	1.5405	0.0064	HOMO→LUMO (0.96)	MLCT/LLCT
	T_1	0.9609	0	HOMO→LUMO (0.95)	^{3}MLCT/^{3}LLCT
Ir2T	S_1	1.6583	0.0048	HOMO→LUMO (0.96)	MLCT/LLCT
	T_1	1.1564	0	HOMO→LUMO (0.96)	^{3}MLCT/^{3}LLCT

OLED Device characterization

The ITO coated glass substrates with a sheet resistance of 15 Ω square^{-1} were consecutively ultrasonicated with acetone/ethanol and dried with nitrogen gas flow, followed by 20 min ultraviolet light-ozone (UVO) treatment in a UV-ozone surface processor (PL16 series, Sen Lights Corporation). Then the samples were transferred to the vacuum deposition system, and the organic layers were deposited at the rates of 0.2-3 Å/s sequentially. After the deposition of organic layers, 8-hydroxyquinolinolato-lithium (Liq) as electron injection layer and aluminum (Al) as cathode layer were deposited with rates of 0.1 and 3 Å/s, respectively by thermal evaporation under 5×10^{-5} Pa. The emitting area of the device is about 0.09 cm^2. The thickness of the deposited films were monitored by an INFICON SQC-310C deposition controller. The current density-voltage-luminance (*J-V-L*), *L-EQE* curves, and electroluminescence spectra were measured using a Keithley 2400 source meter coupled with an absolute EQE measurement system (C9920-12, Hamamatsu Photonics, Japan).

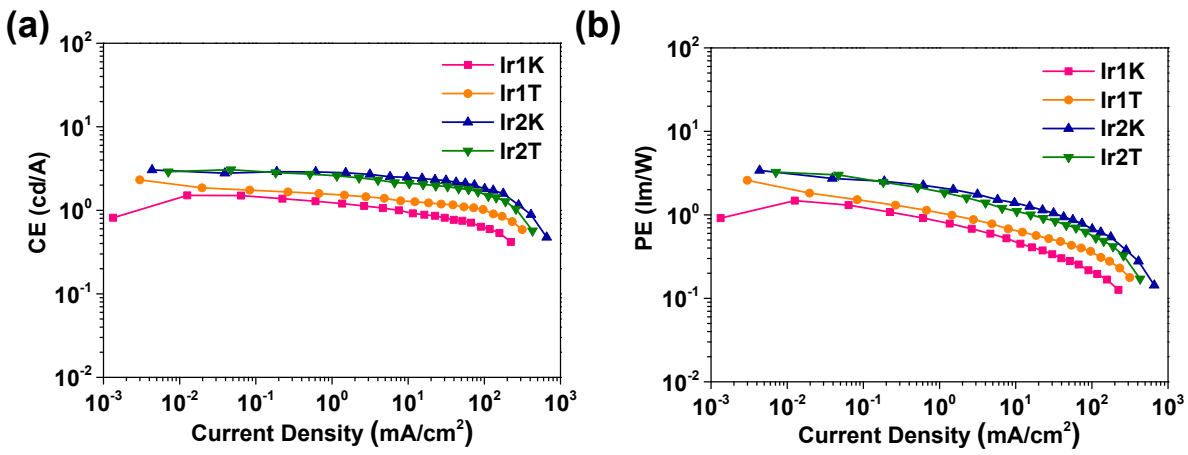

Figure S15. (a) The current efficiency and (b) powder efficiency for device of the iridium complexes **Ir1K**, **Ir1T**, **Ir2K** and **Ir2T**.

NMR and MS spectra

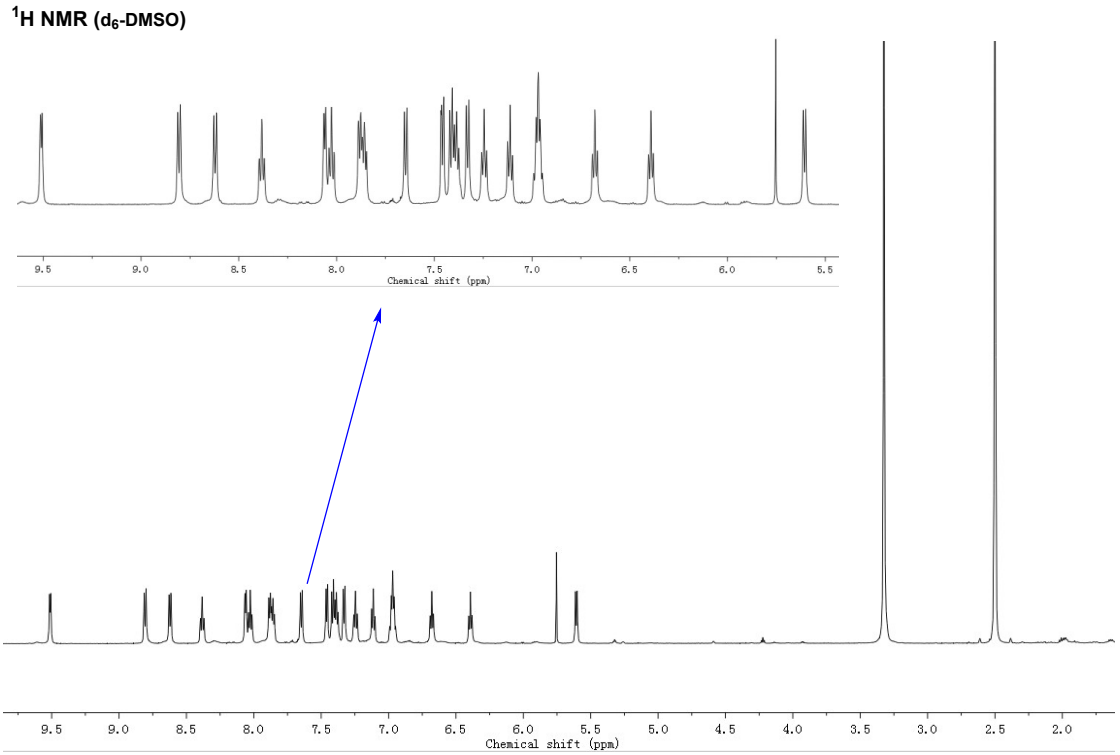

Figure S16. The ^{1}H NMR spectra of the iridium complex **Ir1K**.

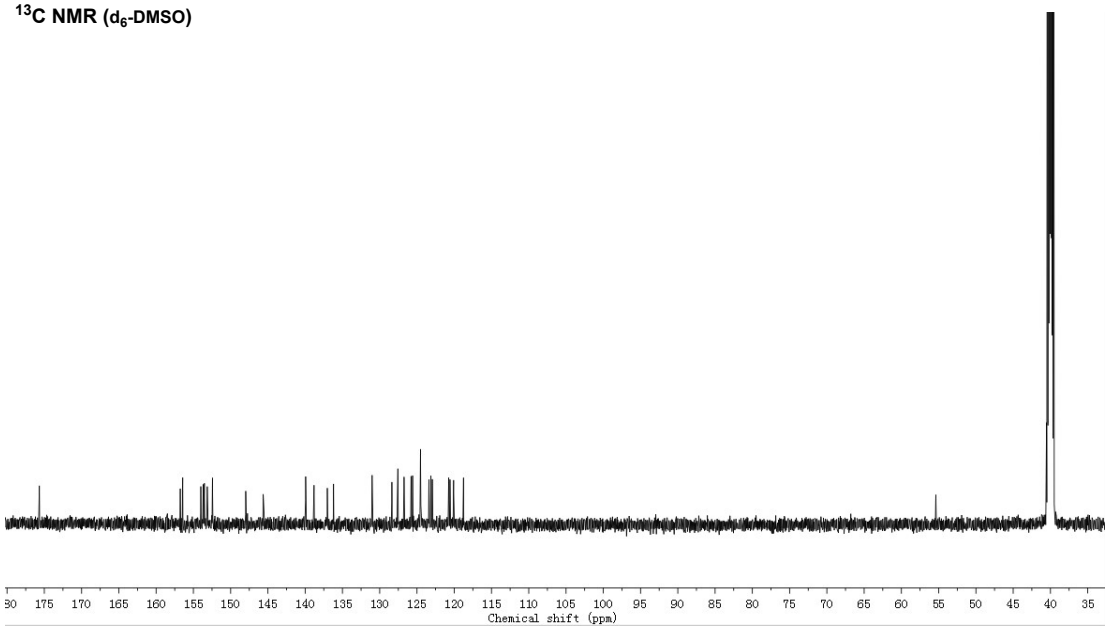

Figure S17. The ^{13}C NMR spectra of the iridium complex **Ir1K**.

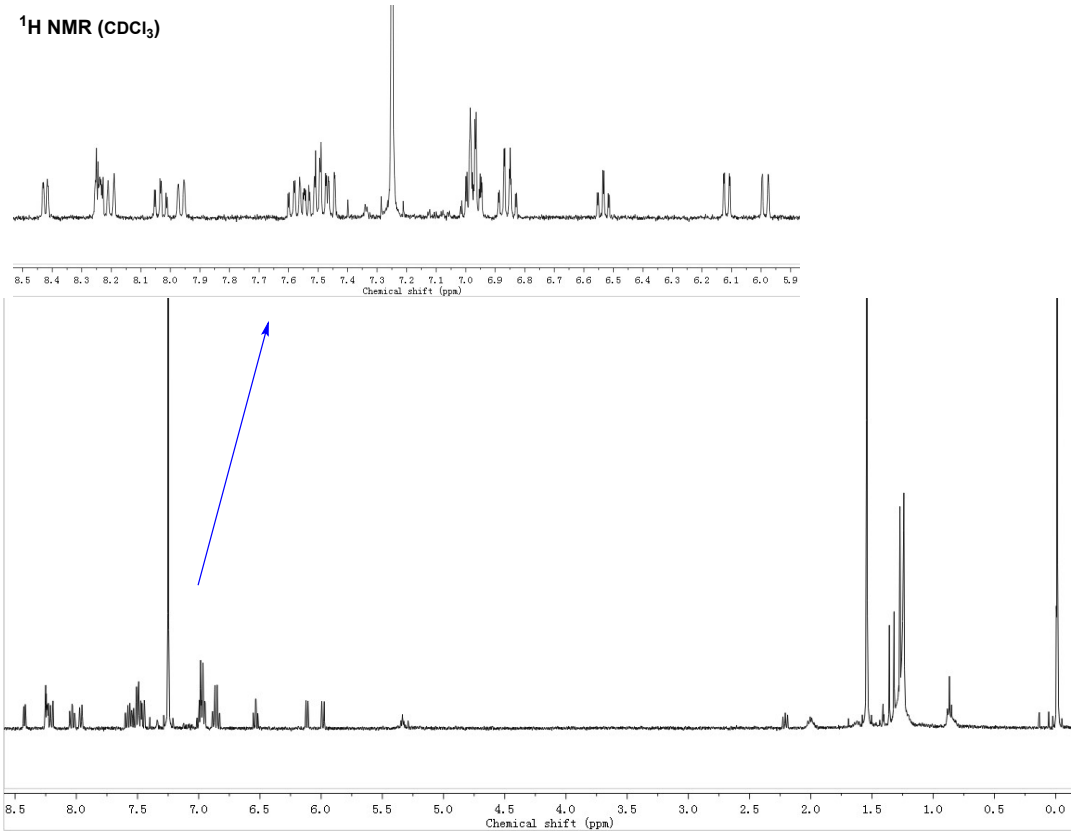

Figure S18. The ^{1}H NMR spectra of the iridium complex **Ir1T**.

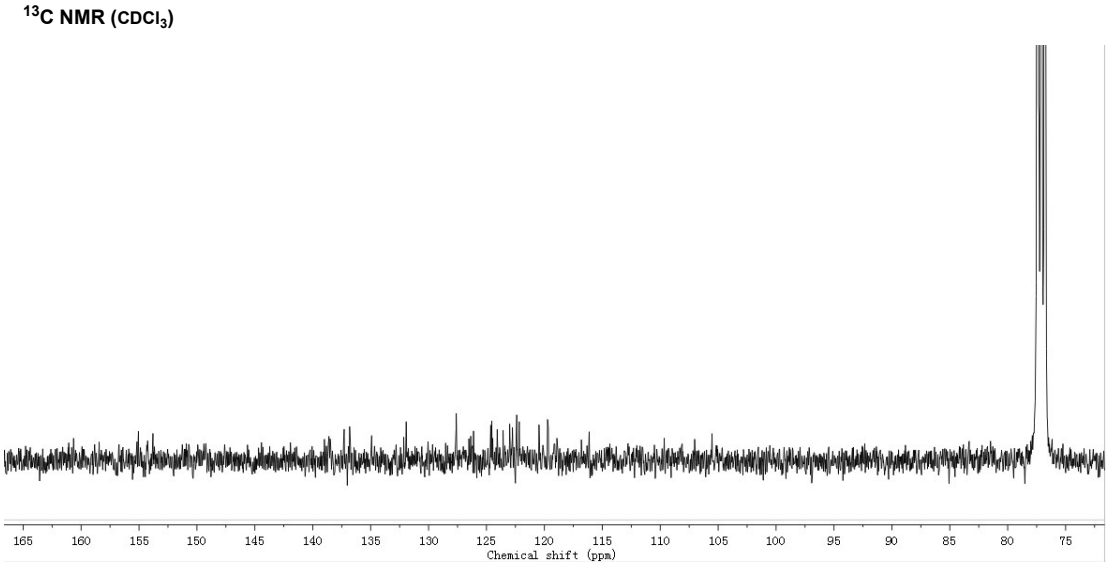

Figure S19. The ^{13}C NMR spectra of the iridium complex **Ir1T**.

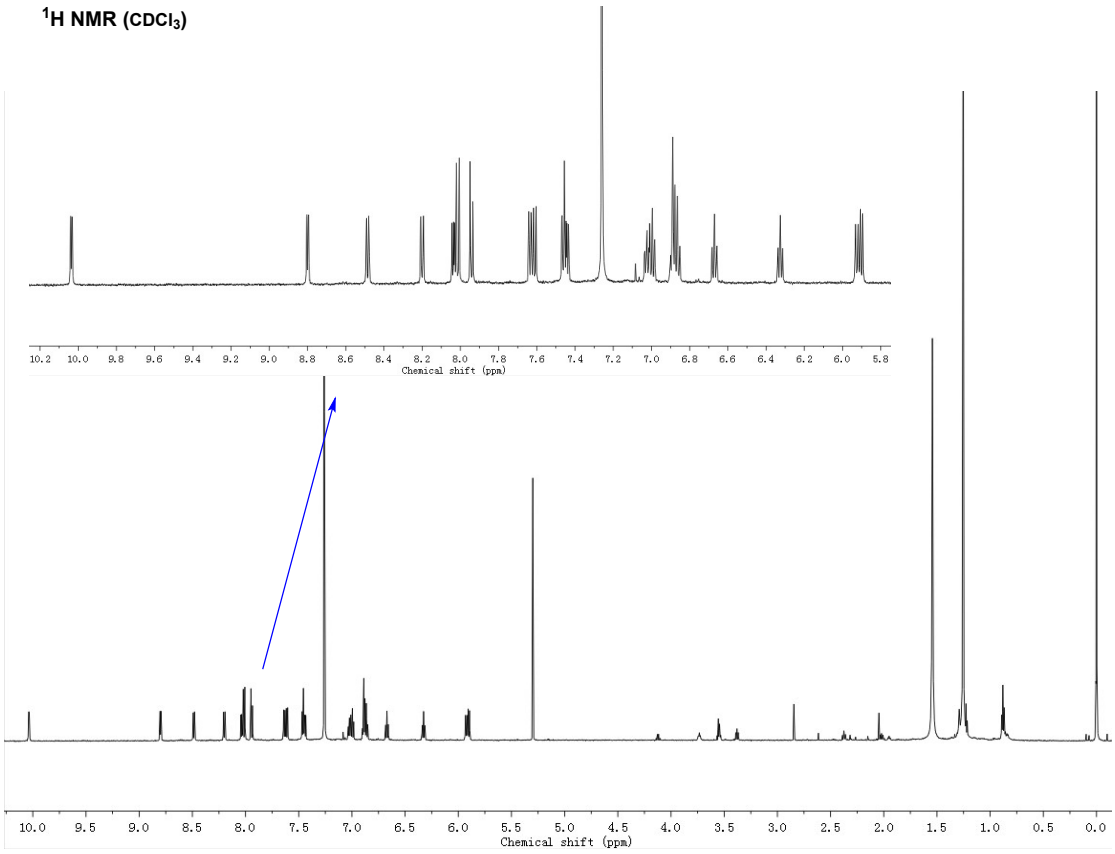

Figure S20. The ^{1}H NMR spectra of the iridium complex **Ir2K**.

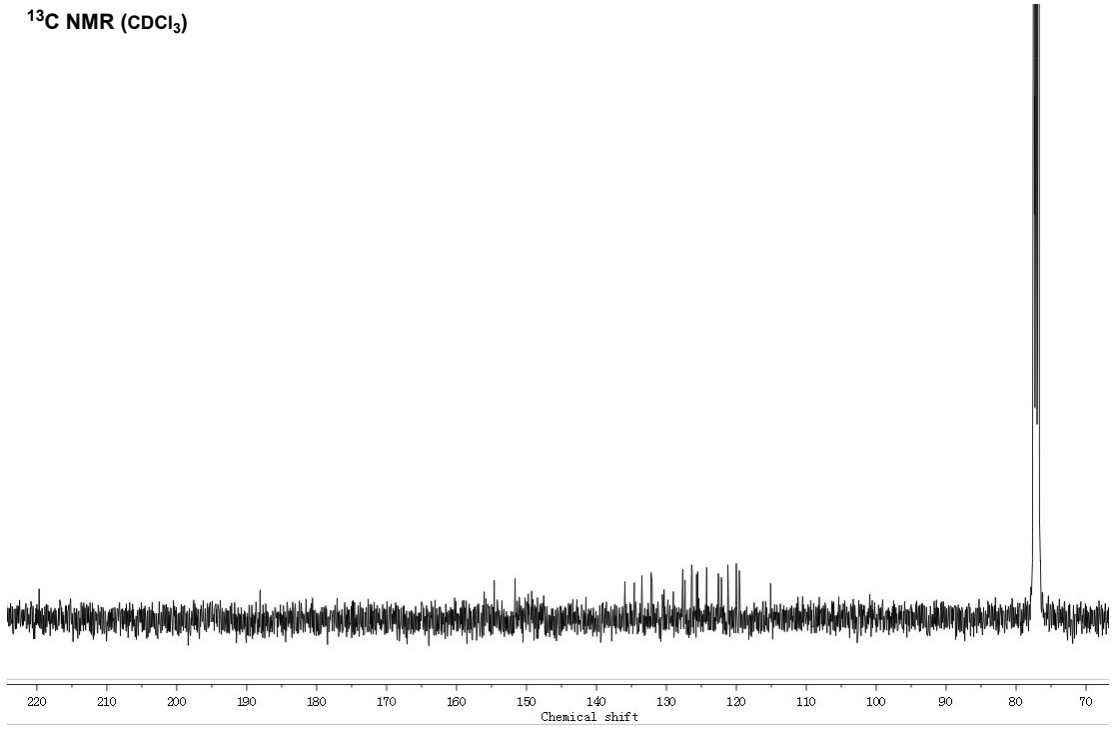

Figure S21. The ^{13}C NMR spectra of the iridium complex **Ir2K**.

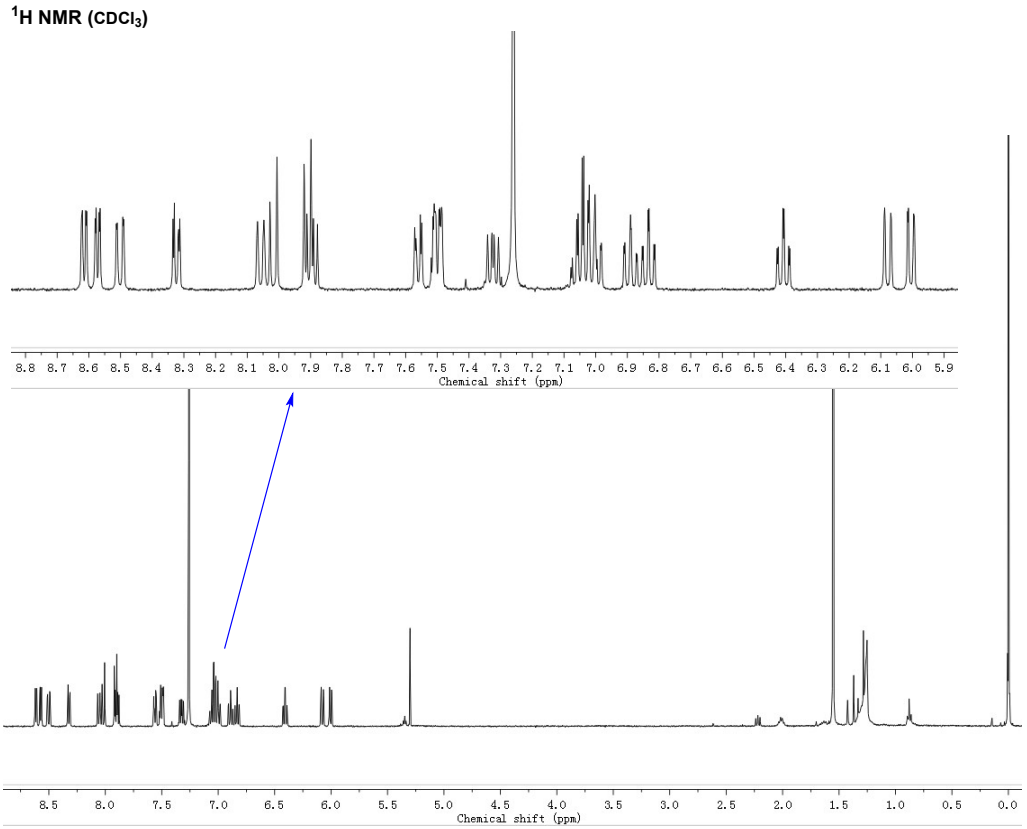

Figure S22. The ^{1}H NMR spectra of the iridium complex **Ir2T**.

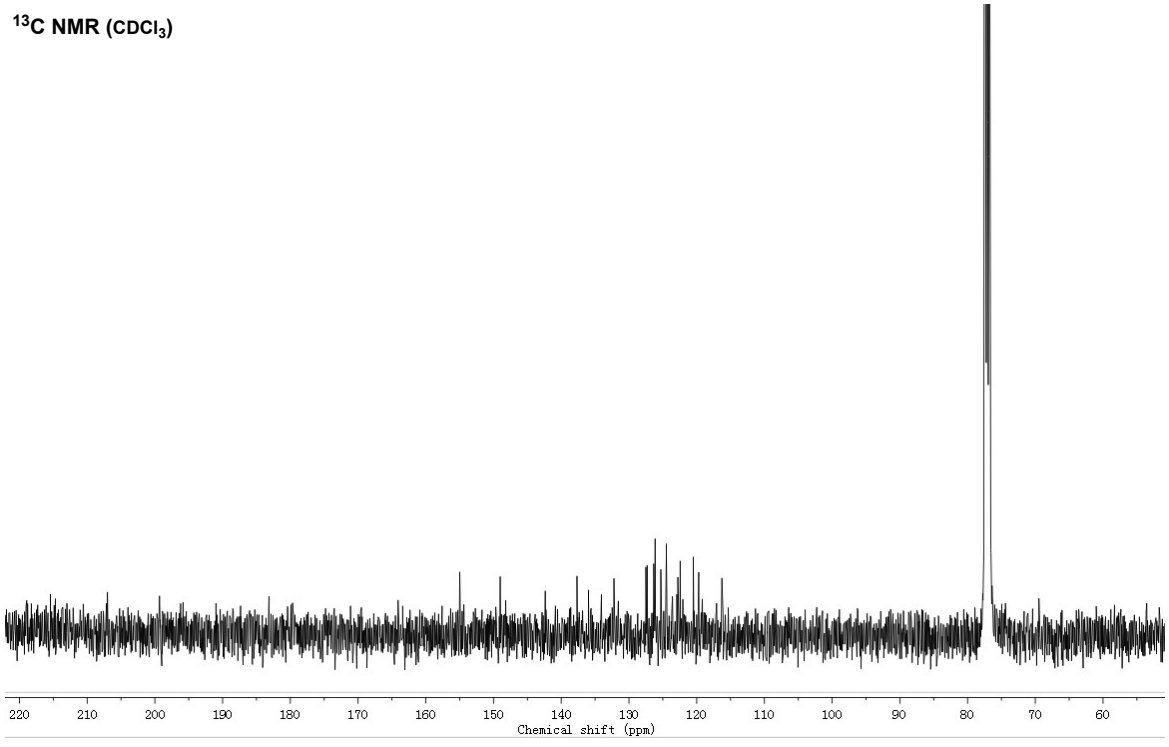

Figure S23. The ^{13}C NMR spectra of the iridium complex **Ir2T**.

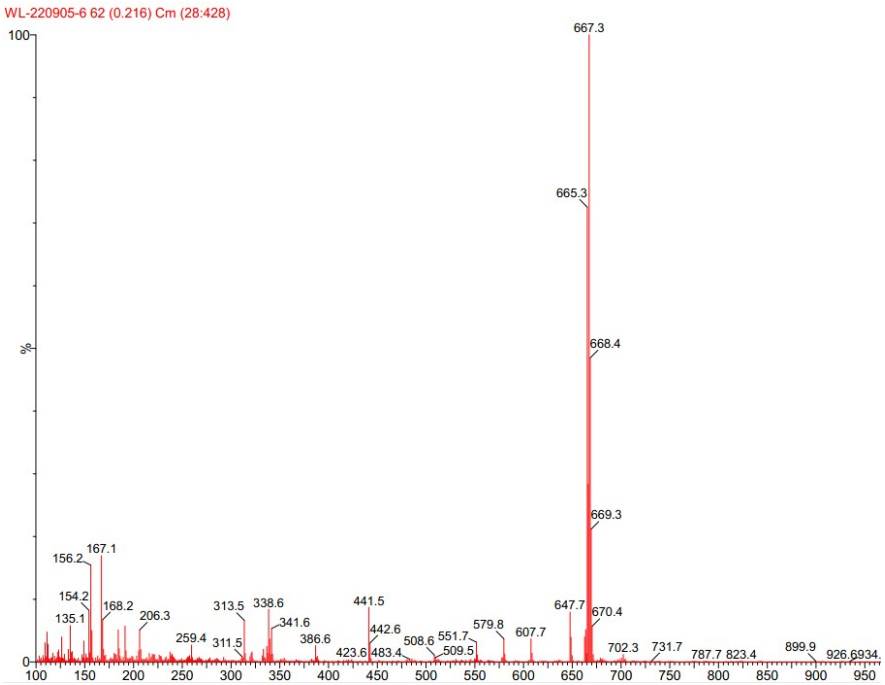

Figure S24. The MS spectra of the iridium complex **Ir1K**.

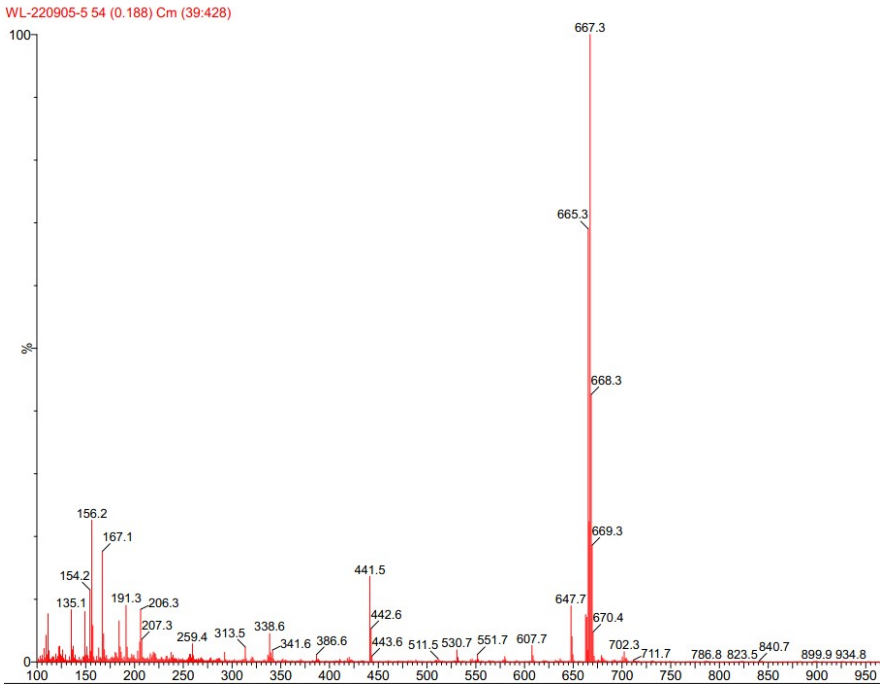

Figure S25. The MS spectra of the iridium complex **Ir1T**.

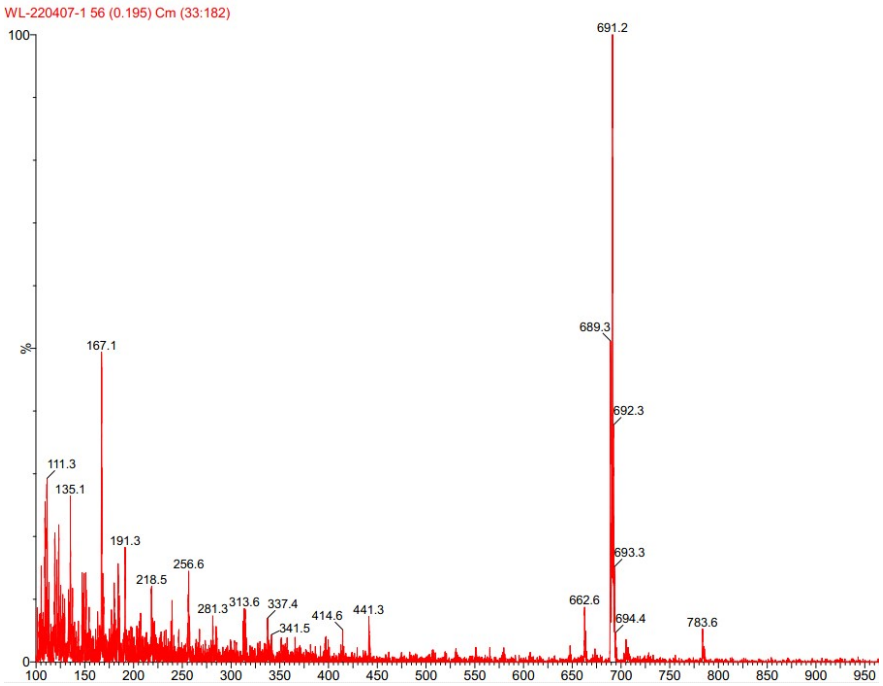

Figure S26. The MS spectra of the iridium complex **Ir2K**.

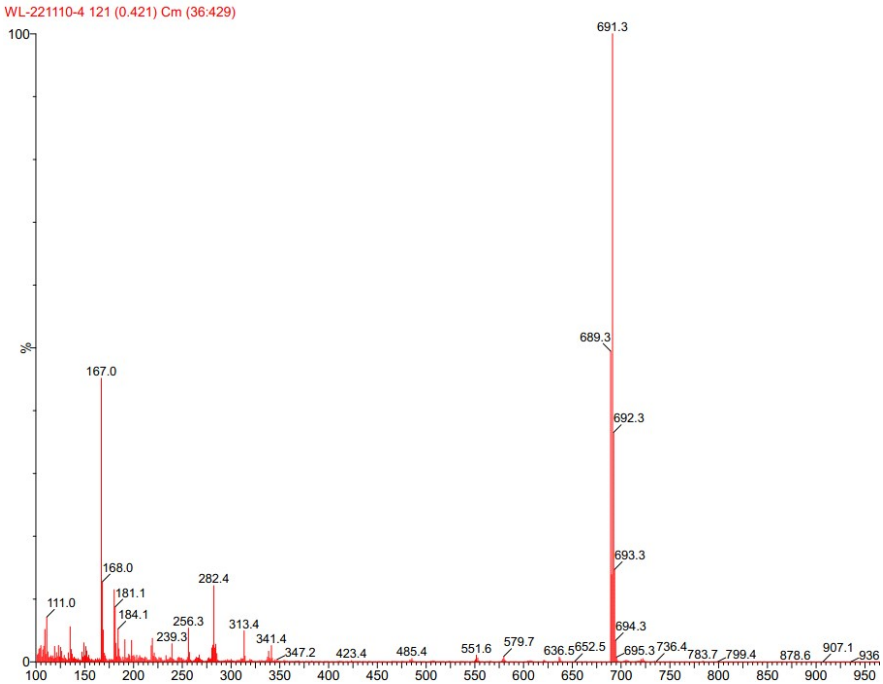

Figure S27. The MS spectra of the iridium complex **Ir2T**.

References

1. C. Shi, H. Huang, Q. Li, J. Yao, C. Wu, Y. Cao, F. Sun, D. Ma, H. Yan, C. Yang, A. Yuan, Three Types of Charged-Ligand-Based Blue–Green to Near-Infrared Emitting Iridium Complexes: Synthesis, Structures, and Organic Light-Emitting Diode Application. *Adv. Optical. Mater.* **2021**, *9*, 2002060.
2. T. Lu, F. W. Chen, Multiwfn: A multifunctional wavefunction analyzer. *J. Comput. Chem.* **2012**, *33*, 580.
3. M. J. Frisch, G. W. Trucks, H. B. Schlegel, G. E. Scuseria, M. A. Robb, J. R. Cheeseman, G. Scalmani, V. Barone, B. Mennucci, G. A. Petersson, H. Nakatsuji, M. Caricato, X. Li, H. P. Hratchian, A. F. Izmaylov, J. Bloino, G. Zheng, J. L. Sonnenberg, M. Hada, M. Ehara, K. Toyota, R. Fukuda, J. Hasegawa, M. Ishida, T. Nakajima, Y. Honda, O. Kitao, H. Nakai, T. Vreven, J. A. Montgomery Jr., J. E. Peralta, F. Ogliaro, M. Bearpark, J. J. Heyd, E. Brothers, K. N. Kudin, V. N. Staroverov, T. Keith, R. Kobayashi, J. Normand, K. Raghavachari, A. Rendell, J. C. Burant, S. S. Iyengar, J. Tomasi, M. Cossi, N. Rega, J. M. Millam, M. Klene, J. E. Knox, J. B. Cross, V.Bakken, C. Adamo, J. Jaram illo, R. Gomperts, R. E. Stratmann, O. Yazyev, A. J. Austin, R. Cammi, C. Pomelli, J. W. Ochterski, R. L. Martin, K. Morokuma, V. G. Zakrzewski, G. A. Voth, P. Salvador, J. J. Dannenberg, S. Dapprich, A. D. Daniels, O. Farkas, J. B. Foresman, J. V. Ortiz, J. Cioslowski and D. J. Fox, Gaussian 09, Revision B.01, Gaussian, Inc., Wallingford CT, **2010**.